Physics of Fluids

Dissipative structures in shear-thickening complex fluids

Cite as: Phys. Fluids **30**, 114104 (2018); https://doi.org/10.1063/1.5051768
Submitted: 12 August 2018 . Accepted: 17 October 2018 . Published Online: 09 November 2018

M. Turcio, A. E. Chávez, J. E. López-Aguilar, R. O. Vargas, A. Capella, and O. Manero

View Online Export Citation CrossMark

ARTICLES YOU MAY BE INTERESTED IN

Numerical study of spheres settling in Oldroyd-B fluids
Physics of Fluids **30**, 113102 (2018); https://doi.org/10.1063/1.5032324

"Phase diagram" for viscoelastic Poiseuille flow over a wavy surface
Physics of Fluids **30**, 113101 (2018); https://doi.org/10.1063/1.5057392

Receptivity of secondary instability modes in streaky boundary layers
Physics of Fluids **30**, 114102 (2018); https://doi.org/10.1063/1.5046136

AIP Publishing

© 2018 Author(s).

Dissipative structures in shear-thickening complex fluids

M. Turcio,[1,2] A. E. Chávez,[1] J. E. López-Aguilar,[1] R. O. Vargas,[3] A. Capella,[4] and O. Manero[2,a)]
[1]*Facultad de Química, Departamento de Ingeniería Química, Universidad Nacional Autonóma de México, Ciudad Universitaria, Coyoacán, CDMX 04510, Mexico*
[2]*Instituto de Investigaciones en Materiales, Universidad Nacional Autónoma de México, A.P. 70-360, México, CDMX 04510, Mexico*
[3]*ESIME Azcapotzalco, Instituto Politécnico Nacional, Avenida de las Granjas No. 682, Colonia Santa Catarina, Delegación Azcapotzalco, México, CDMX 02250, Mexico*
[4]*Instituto de Matemáticas, Universidad Nacional Autónoma de México, México, CDMX 04510, Mexico*

(Received 12 August 2018; accepted 17 October 2018; published online 9 November 2018)

The main objective of this work is to demonstrate that non-local terms of the structure variable and shear-stress is a sufficient condition to predict multiple bands in rheologically complex fluids, i.e., shear-thickening fluids. Here, shear bands are considered as dissipative structures arising from spatial instabilities (Turing patterns) rather than the classical mechanical instability. In the present analysis, a monotonic relation between shear-stress and shear-rate holds. The formation of banded patterns is discussed for shear-thickening fluids with a model that consist of an upper-convected Maxwell-type constitutive equation coupled to an evolution equation for the structure variable, in which both non-local terms of the stress and of the structure variable are included (non-local Bautista-Manero-Puig model). The Turing mechanism is used to predict a critical point for primary instabilities (stable bands), while the amplitude formalism is used to predict secondary instabilities and marginal curves. *Published by AIP Publishing.* https://doi.org/10.1063/1.5051768

I. INTRODUCTION

In 1952, Allan Turing proposed that diffusion can cause instabilities in an otherwise stable reaction system (Turing, 1952), leading to a break-up of spatial symmetry and the development of spatial structures known as Turing patterns. Such structures were given much attention in the context of non-equilibrium systems, named therein "dissipative structures" (Nicolis and Prigogine, 1977; Manneville, 1990; and Kim and Park 1993), where the Turing mechanism has been associated with the presence of interacting species having different mobilities and cooperative interactions (Walgraef, 1996). Close to the instability threshold, Turing patterns may display secondary instabilities, causing complex spatio-temporal phase dynamics (Peña Pellicer, 2002; Gambino *et al.*, 2012; and Walgraef, 1996). Such complex behaviors can be qualitatively described via weak non-linear techniques, namely, amplitude equations which depend on the primary instability rather than on the particular model used (Manneville, 1990; van Beijeren and Ernst, 1994; and Walgraef, 1996). Such linear stability analysis and non-linear techniques have been used previously in the context of shear-banding instabilities in granular materials (Shukla and Alam, 2013) and in elastic solids (Walgraef, 1996), leading to a Landau-type amplitude equations.

Non-local spatial terms are neglected in homogeneous flow regimes, although their contribution is important to obtain stable solutions in some finitely extensible nonlinear elastic (FENE) models (El-Kareth and Leal, 1989). In addition, the incorporation of polymer diffusivity into constitutive equations has been of considerable interest, motivated by the fact that there are fundamental difficulties with the existence of solutions and convergence of numerical algorithms in the simulation of complex flows of non-Newtonian fluids when these effects are neglected (Öttinger, 1992 and Bhave *et al.*, 1991).

In recent years, non-local spatial terms have been given attention in the study of shear-banding in systems where, given the strong feedback between the structure of the fluid and the flow dynamics, a spatially inhomogeneous state with regions of different mechanical properties coexist for a fixed level of shear-stress (or shear-rate) (Aradian and Cates 2005; Wilson and Fielding, 2006; and Fielding and Wilson, 2010). In some mesoscopic models, the instabilities come from the feedback between the shear-stress and the physical structure of the micelles, i.e., through reaction-like interactions (Cates, 1987 and Cates and Fielding, 2010), and the tube dynamics of elongated structures (Doi and Edwards, 1989 and Mead *et al.*, 1998). These models are extremely difficult, and even untractable in the non-linear flow regime (Fardin and Lerouge, 2012). Nevertheless, shear-banding is considered to arise from a thermodynamic-like, mechanical instability, inherent to a non-monotonic relation between shear-stress and shear-rate in the constitutive model (Aradian and Cates, 2005; Wilson and Fielding, 2006; Fardin and Lerouge, 2012; Porte *et al.*, 1997; Bautista *et al.*, 2002; 2007; Manero *et al.*, 2007; and García-Sandoval *et al.*, 2012). Such instability is of spinodal-type, which determines a shear-stress (or shear-rate) plateau and fixes the possible coexisting states in question. Therefore models with a non-monotonic relation between shear-stress and shear-rate form two stable bands (with a flat interface), determined by the stress plateau.

The classical shear-banding phenomenon described before was motivated by time- and space-average measurements. Nevertheless, experiments with enhanced temporal and spatial resolution showed fluctuations to the classical picture

a)Electronic mail: manero@unam.mx

in micellar systems (Fardin and Lerouge, 2012; Lerouge and Berret, 2010; and Olmsted, 2008). Such fluctuations have been reported at the local scale, i.e., by flow birefringence where the induced bands are shown to have a complex spatio-temporal behavior, while velocity profiles obtained by nuclear magnetic resonance (NMR) demonstrated that the band-interface may exhibit regular and erratic motions (Manneville, 2008; Fardin *et al.*, 2010; and Fardin and Lerouge, 2012). Other complex phenomena, such as intermittent band nucleation, have also been observed (Fardin *et al.*, 2015; Fardin and Lerouge, 2012; and Lerouge *et al.*, 2008). Also, velocimetry experiments have revealed a strong feedback between the boundary conditions and the bulk dynamics, without distinguishing the proper relation between these effects (Fardin and Lerouge, 2012). These complex behaviors are known features of dissipative structures (Manneville, 1990; Peña Pellicer, 2002; and Walgraef, 1996), and thus shear-banding and rheo-chaos are potential manifestations of non-local instabilities in complex fluids.

Besides to all these complex phenomena, shear-thickening fluids present additional complications (Olmsted, 2008), most of them emerging from the fact that the mechanics of the thickening process are not well understood (Mitkin and Thofanous, 2017; Olmsted, 2008; Townsend and Wilson, 2017; and Vázquez-Quesada *et al.*, 2017). Some kinetic models propose that thickening behavior of material comes from repulsive interactions and contact forces between the particles within the fluid (Townsend and Wilson, 2017), while continuous models discuss the different types of shear-thickening, i.e., continuous and discontinuous (Townsend and Wilson, 2017 and Vázquez-Quesada *et al.*, 2017). In the latter, the fluid can form multiple bands due to a discontinuity in the viscosity (Vázquez-Quesada *et al.*, 2017).

In this work, attention is given to the prediction of multiple bands in fluids with monotonically increasing flow-curves. The non-local spatial contributions are studied and sufficient conditions to induce stable spatial patterns in rheologically complex fluids are given. These fluids are modeled with a constitutive equation containing a stress-deformation rate relation coupled with an evolution equation describing the fluid internal structure within a tensorial generalized scheme. The analysis covers shear-thickening fluids flowing in an unbounded simple shear. A weak non-linear technique (amplitude formalism) is then used to predict secondary instabilities and a phase equation is obtained, allowing qualitative comparison with experimental results reported in the literature.

II. THE BMP MODEL

Flow phenomena in complex fluids have been analyzed with the Bautista-Manero-Puig (BMP) model (Bautista *et al.*, 1999). This rheological model couples non-linear viscoelastic effects with structural parameters of the fluid, consisting in the upper-convected Maxwell equation (1) and a kinetic equation for structural changes due to the flow (2). The tensorial form of this system is:

$$\boldsymbol{\sigma} + \frac{1}{G\varphi}\overset{\triangledown}{\boldsymbol{\sigma}} = \frac{2}{\varphi}\dot{\boldsymbol{\gamma}}, \tag{1}$$

$$\frac{d\varphi}{dt} = \frac{\varphi_0 - \varphi}{T} + k(\varphi_\infty - \varphi)\boldsymbol{\sigma} : \dot{\boldsymbol{\gamma}}, \tag{2}$$

$$\overset{\triangledown}{\boldsymbol{\sigma}} = \frac{d\boldsymbol{\sigma}}{dt} - \left(\boldsymbol{L}\cdot\boldsymbol{\sigma} + \boldsymbol{\sigma}\cdot\boldsymbol{L}^T\right). \tag{3}$$

Here $\frac{d}{dt}$ is the material-time derivative, $\dot{\boldsymbol{\gamma}}$ is the symmetric part of the velocity-gradient tensor $\boldsymbol{L}$, G is the elastic relaxation modulus, φ represents the fluidity (inverse of the viscosity η), φ_0 and φ_∞ are the fluidities at zero and high shear-rate, respectively, T is the characteristic time of structural reformation, and k is a kinetic parameter that modulates stress dissipation. When the parameter k is constant, the BMP model can predict a great variety of rheological phenomena, such as non-Newtonian viscosity, viscoelasticity, and thixotropy for complex fluids (Bautista *et al.*, 1999).

The original BMP model has been extended to analyze shear-banding in micellar fluids (Bautista *et al.*, 2002), wherein the parameter k is expanded to a first-order dependence on the second invariant of $\dot{\boldsymbol{\gamma}}$, yielding a cubic relation of the fluidity with the shear-rate. The cubic BMP model predicts a non-monotonic relation between the shear-stress and the shear-rate, resulting in a region of negative slope in the flow-curve, which can be analyzed through spinodal decomposition, leading to formation of shear-bands. The predictions of the cubic BMP model have been extensively studied in the context of shear-banding of micellar fluids (Bautista *et al.*, 2002 and Manero *et al.*, 2007).

The extended irreversible thermodynamics formalism provides a fundamental grounding to the BMP model (Manero *et al.*, 2007 and García-Sandoval *et al.*, 2012); this derivation shows that the model includes inhomogeneous, non-local terms when a diffusive current is included in the formulation, allowing couplings between the stress, structure, and their spatial dependence. The resulting equations are:

$$\boldsymbol{\sigma} + \frac{1}{G\varphi}\overset{\triangledown}{\boldsymbol{\sigma}} = \frac{2}{\varphi}\dot{\boldsymbol{\gamma}} + \beta_2'(\nabla\boldsymbol{J})^S, \tag{4}$$

$$\frac{d\varphi}{dt} = \frac{\varphi_0 - \varphi}{T} + k(\varphi_\infty - \varphi)\boldsymbol{\sigma} : \dot{\boldsymbol{\gamma}} + \beta_0'\nabla\cdot\boldsymbol{J}, \tag{5}$$

$$\boldsymbol{J} + \tau_1\frac{d\boldsymbol{J}}{dt} = -D_F\nabla c + \beta_0\nabla\varphi + \beta_2\nabla\cdot\boldsymbol{\sigma}, \tag{6}$$

where $(\nabla\boldsymbol{J})^S$ stands for the symmetric part of $\nabla\boldsymbol{J}$, the mass flux, τ_1 is a relaxation time for the mass flux, D_F is the Fickean diffusion coefficient, c is the local equilibrium concentration, and β_0, β_0', β_2, and β_2' are so far phenomenological parameters. Beyond the local equilibrium hypothesis, these equations predict flow-induced concentration changes coupled with the spatial distribution of stress and structure within the fluid. Such couplings describe how the mass flux gradients affect the stress distribution [second term on the right-hand side of Eq. (4)], how the mass flow changes the local structure of the fluid and vice versa [third term on the right-hand side of Eq. (5) and the second term in same side of Eq. (6), respectively], and how stress in the material causes a diffusive mass flux [third term on the right-hand side of Eq. (6)].

Non-local terms can give rise to shear-band formation in complex fluids, where bands arise from spatial instabilities rather than the classical thermodynamic-like instability. In the context of the present work, the resulting bands are known as dissipative structures. In order to keep the Introduction brief, the derivation of the model is carried out in Appendix A for the

particular case of constant spatial coefficients, while allowing a variable relaxation time.

A. Non-local BMP model

For simple-shear flow (where x is the direction of the macroscopic flow velocity, y is the direction of the velocity-gradient, and z is the direction of the vorticity) with constant spatial coefficients and with the restrictions imposed for this particular case, the following equations are obtained:

$$\mathrm{T}_{xy} = \sigma_{xy} + \eta_s\dot{\gamma}, \tag{7}$$

$$\frac{\partial\sigma_{xy}}{\partial t} = -G\varphi\sigma_{xy} + \dot{\gamma}G + \frac{GD_0}{\varphi_\infty}\nabla^2\varphi + D_1\nabla^2\sigma_{xy}, \tag{8}$$

$$\frac{\partial\varphi}{\partial t} = \frac{\varphi_0 - \varphi}{T} + k(\varphi_\infty - \varphi)\sigma_{xy}\dot{\gamma} + D_0\nabla^2\varphi, \tag{9}$$

$$\frac{\partial N_1}{\partial t} = -G\varphi N_1 + 2\dot{\gamma}\sigma_{xy} + \frac{GD_0}{\varphi_\infty}\nabla^2\varphi, \tag{10}$$

$$\frac{\partial N_2}{\partial t} = -G\varphi N_2 + \frac{GD_0}{\varphi_\infty}\nabla^2\varphi. \tag{11}$$

In this version of the model, we split the total shear-stress T_{xy} into a non-uniform viscoelastic micellar contribution σ_{xy} added to a Newtonian solvent contribution with viscosity η_s, where $\dot{\gamma}$ is the shear-rate and the first and second normal-stress differences are $N_1 = \sigma_{xx} - \sigma_{yy}$ and $N_2 = \sigma_{yy} - \sigma_{zz}$, respectively.

In these equations, the constants D_i ($i = 0, 1$) are the spatial coefficients related to the mobility (spatial displacement rate) of the corresponding variables. Keeping in mind that rheometric flows require that $Re \to 0$, advective terms may be neglected in the equations and the main mechanism of transport within the fluid is diffusion. Note that advective terms may not be neglected when dealing with high-Re or high-W flows since such terms lead to turbulence-like instabilities (Fardin and Lerouge, 2012 and Larson, 1992).

In the case of micellar fluids, the momentum is transported by diffusion of the micelles through the solvent, leading to structural changes in the micelles; hence, spatial variations on both stress and fluidity (representative of the structure of the fluid) must be considered in the model. Also, note that only one cross-spatial term is considered, i.e., the fluidity non-local term in Eq. (8). This term shows explicitly the cooperative interactions between the fluid structure and the shear-stress. It will be shown that this term is needed in the subsequent definition of the Turing space. If a cross-spatial term were to be added to the fluidity equation, it had to follow Onsager's reciprocal relations (Nicolis and Prigogine, 1977). In this set of equations, the governing variables are the shear-stress and the fluidity, σ_{xy} and φ, respectively; thus, the shear-rate $\dot{\gamma}$ can be treated as a parameter of the dynamics. Finally, it is important to mention that normal-stress differences, Eqs. (10) and (11), decouple from the stress equation and its behavior can be inferred from σ_{xy} and φ. Furthermore, Eq. (10) shows that the natural equilibrium value of N_1 is related to σ_{xy}^2, while, from Eq. (11), the equilibrium value for N_2 is zero. Hence, in the following, attention will be given to the stress and fluidity equations, while the normal-stress differences will be neglected.

In the BMP model, the relation between the fluidity, the relaxation time τ, and the micellar length n is $\tau = \frac{1}{G\varphi} = \tau_0\left(\frac{\mathrm{n}}{\mathrm{n}_0}\right)$, where τ_0 and n_0 are the relaxation time and the micellar length when $\varphi = \varphi_0$, respectively. Substitution of this relation into the evolution equation for the fluidity [Eq. (9)] yields an equation that can be expressed in terms of the average micellar length n, which is a microstructural variable associated with the fluidity. The physical interpretation is that the micellar length follows an evolution equation related to breakage and reformation processes of the micelles. The internal-structure equation itself is coupled to the total stress, which contains the non-local micellar contribution.

For the subsequent treatment, it is convenient to use the following non-dimensional variables, i.e.:

$$t^* = G\varphi_\infty t, \tag{12}$$

$$\varphi^* = \frac{\varphi}{\varphi_\infty}, \tag{13}$$

$$\sigma_{xy}^* = \frac{\sigma_{xy}}{G}, \tag{14}$$

$$\nabla^{*2} = \frac{D_1}{G\varphi_\infty}\nabla^2. \tag{15}$$

Non-dimensional variables are written with a superscript $*$. In Eq. (12), the characteristic time is defined as the inverse of the viscoelastic time at a high shear-rate ($G\varphi_\infty$), and φ_∞ is the characteristic fluidity in Eq. (13). The shear-stress in Eq. (14) is normalized using the elastic relaxation modulus, and in Eq. (15) the square of the characteristic length, associated to the non-local variations of shear-stress, is used to form the non-dimensional Laplacian operator.

The resulting non-dimensional equations are:

$$\frac{\partial\sigma_{xy}^*}{\partial t^*} = -\varphi^*\sigma_{xy}^* + W + D^*\nabla^{*2}\varphi^* + \nabla^{*2}\sigma_{xy}^*, \tag{16}$$

$$\frac{\partial\varphi^*}{\partial t^*} = T^*(\varphi_0^* - \varphi^*) + K^*(1 - \varphi^*)W\sigma_{xy}^* + D^*\nabla^{*2}\varphi^*. \tag{17}$$

Non-dimensional terms arising are the structural time $T^* = \frac{1}{G\varphi_\infty T}$, a structural stress $K^* = Gk$, a spatial coefficient $D^* = \frac{D_0}{D_1}$, and the Weissenberg number $W = \frac{\dot{\gamma}}{G\varphi_\infty}$. For simplicity, $*$ superscripts will be omitted hereafter.

III. TURING SPACE FOR THE NON-LOCAL BMP MODEL

In his famous paper (Turing, 1952), Alan Turing proposed that a system of chemical substances, called morphogens, may react together and diffuse through embryos' tissues, and that the reaction-diffusion interactions are sufficient to account for the morphogenesis phenomena of the tissues; that is, although originally spatially homogeneous, the blastula may develop different tissues (spatial structures) due to an instability triggered by random spatial disturbances (Turing, 1952). He considered that the dynamical equations of the morphogens had the form:

$$\frac{\partial\phi}{\partial t} = f(\phi,\psi) + C_1\nabla^2\phi,$$

$$\frac{\partial\psi}{\partial t} = g(\phi,\psi) + C_2\nabla^2\psi,$$

where ϕ and ψ are the morphogens concentrations at time t, $f(\phi, \psi)$ and $g(\phi, \psi)$ are the corresponding chemical reaction terms, and $C_1\nabla^2\phi$ and $C_2\nabla^2\psi$ account for the diffusion of the morphogens through the tissue.

Following Turing's idea (Turing, 1952), first note that the right-hand side of Eqs. (16) and (17) can be split into two contributions; one arising from the "reaction" terms $f(\sigma, \varphi) = -\varphi\sigma + W$ and $g(\sigma, \varphi) = T(\varphi_0 - \varphi) + K(1 - \varphi)W\sigma$, and the second one containing the "diffusion" terms, $D\nabla^2\varphi + \nabla^2\sigma_{xy}$ and $D\nabla^2\varphi$, respectively. Now, homogeneous equilibrium solutions are defined in such a way that the "reaction" terms are cancelled, i.e., $f(\sigma_E, \varphi_E) = 0$ and $g(\sigma_E, \varphi_E) = 0$; hence,

$$\sigma_E = \frac{W}{\varphi_E}, \tag{18}$$

$$\varphi_E = \frac{T\varphi_0 - KW^2}{2T} + \sqrt{\left(\frac{T\varphi_0 - KW^2}{2T}\right)^2 + \frac{KW^2}{T}}, \tag{19}$$

where the subscript E indicates an equilibrium value. Note that in Eq. (19), the second root of the quadratic expression for φ has been neglected; such a root yields a negative value for the fluidity and has no physical meaning (Bautista *et al.*, 1999).

In order to include the non-local effects, spatial perturbations of the steady-state solutions are proposed (Peña Pellicer, 2002), i.e., $\sigma = \sigma_E + \hat{\sigma}$ and $\varphi = \varphi_E + \hat{\varphi}$. Inserting these expressions in (16) and (17) and keeping only the linear contributions of the perturbation scheme (linear terms account for the pattern formation), the perturbation equations are:

$$\frac{\partial}{\partial t}\boldsymbol{u} = \boldsymbol{l}\cdot\boldsymbol{u}, \tag{20}$$

where:

$$\boldsymbol{u} = \begin{pmatrix}\hat{\sigma}\\ \hat{\varphi}\end{pmatrix}, \tag{21}$$

$$\boldsymbol{l} = \begin{pmatrix}-\varphi_E + \nabla^2 & -\sigma_E + D\nabla^2\\ KW(1-\varphi_E) & -T - KW\sigma_E + D\nabla^2\end{pmatrix}. \tag{22}$$

Note here that the zeroth-order terms in Eq. (20) vanish identically because of the definition of σ_E and φ_E. Equation (20) represents the evolution of spatial perturbations to the stable homogeneous solutions. If the perturbations disappear, then the homogeneous solution is recovered and the fluid stabilizes to a single phase. On the other hand, if perturbations destabilize the homogeneous solution, the spatial symmetry is lost and the system evolves into a multiphase state, where spatial patterns are formed. Pattern formation depends on both the geometry of the cell of fluid and boundary conditions.

The stability of the "reaction" systems requires negative eigenvalues of the linear operator (22) in the absence of non-local terms (Ponce, 2013), leading to the following conditions:

$$\varphi_E + T + KW\sigma_E > 0, \tag{23}$$

$$T\varphi_E + KW\sigma_E > 0. \tag{24}$$

Since σ_E and φ_E are positive for all values of W [see Eqs. (18) and (19)], these conditions are trivially fulfilled because they require that characteristic times of structural construction (T) and destruction (K) to be positive; hence, the BMP model produces stable homogeneous values of φ_E and σ_E for all W. These conditions are also applicable to the cubic BMP model since the expansion of K as a function of W affects the equilibrium solutions but not the linear stability conditions represented by inequalities (23) and (24). Hence, the whole non-monotonic flow-curve, related to the classical shear banding phenomenon, remains stable for all values of W in the local model.

As mentioned above, patterns might be bands of different properties resembling shear-bands. These are one-dimensional structures with variations along their normal direction y, and hence, non-local terms will follow an equation describing plane waves, that is,

$$\boldsymbol{u} = \boldsymbol{u}_0 e^{\omega t} e^{iqy}. \tag{25}$$

Here, ω is the eigenvalue (frequency) corresponding to the wave number q and $\boldsymbol{u}_0$ is the eigenvector associated to the unstable mode. Note that the sign of ω determines the time behavior of the perturbations allowing three situations: if $\omega < 0$, perturbations decrease with time and disappear as $t \to \infty$, and therefore the system is stable. The opposite situation occurs when $\omega > 0$, for which perturbations grow with time and the system becomes unstable. Finally, if $\omega = 0$, perturbations remain constant over time, and the system is marginally stable. For this reason, the eigenvalue ω accounts for the growth rate, as defined elsewhere (Fielding and Wilson, 2010).

Stability analysis of the linear operator (22) leads the following condition for instability, namely, the dispersion relation (Ponce, 2013):

$$Dq^4 + [D\varphi_E + T + KW\sigma_E + DKW(1-\varphi_E)]q^2 + \varphi_E + KW\sigma_E < 0. \tag{26}$$

Note that the left-hand side of this inequality represents an upward parabola (convex curvature) in q^2, namely, $h(q^2)$. Condition (26) is fulfilled when the minimum of $h(q^2)$ is negative, and therefore, satisfying the inequality (26) requires the term $1 - \varphi_E$ to be negative. Since the fluidity is normalized with respect to the fluidity at high shear-rates [see Eq. (13)], this condition is fulfilled for shear-thickening fluids. In addition, it is also required that the magnitude of the term $DKW(1 - \varphi_E)$ be sufficiently large. At low W, the term may be small, and it is also small for large W since $\varphi_E \to 1$. Hence, the instability occurs only for intermediate values for W; this result qualitatively agrees with experimental shear-banding data (Fardin *et al.*, 2010 and Fardin and Lerouge, 2012). An important issue arises: the presence of the cross-spatial term, $D\nabla^2\hat{\varphi}$, in Eq. (8), corresponding to the cooperative interactions between the fluid-structure and the shear-stress, is a necessary condition for the onset of instabilities of the Turing-type for shear-thickening fluids. The cross-spatial term appears in the dispersion relation (26) as the fourth term in the quadratic part of this condition. Since the spatial coefficients are considered positive, the cross-spatial term is the only possible negative contribution in condition (26), and hence, it is necessary for the instability to arise.

Furthermore, according to Eq. (26), there are values of the Weissenberg number, W, for which the minimum of $h(q^2)$ is either positive, zero, or negative. Positive values of the minimum of $h(q^2)$ do not form patterns, while negative values of

the minimum fulfill the condition for spatial instability. The zero value represents the transition between spatial homogeneous and inhomogeneous flow-regime, i.e. the bifurcation point, defining the critical Weissenberg number W_c for the pattern formation. Another important result arises: the minimum of $h(q^2)$ represents the critical wave number q_c (the fastest mode when unstable), and it depends on W. The spatial pattern formed may depend on the value of W relative to W_c, because the difference $W - W_c$ represents how fast the perturbations grow compared to their maximum possible rate.

Finally, when condition (26) is fulfilled, there are two values of q^2 for which $h(q^2)$ is zero (q_-^2 and q_+^2, respectively) defined as:

$$q_\pm^2 = -\frac{D\varphi_E + T + KW\sigma_E + DKW(1-\varphi_E)}{2D} \pm \sqrt{\left(\frac{D\varphi_E + T + KW\sigma_E + DKW(1-\varphi_E)}{2D}\right)^2 - \frac{T\varphi_E + KW\sigma_E}{D}}. \tag{27}$$

Note that both q_-^2 and q_+^2 are positive, signaling the interval known as the Turing space; the possible lengths of the patterns are bounded by these values. The bifurcation points correspond to the values of W for which $q_+ = q_-$, i.e. the points for which the minimum of $h(q^2)$ is zero, signaling the beginning and the end of the banded states. Additionally, q_-^2 and q_+^2 depend also on the W, so the Turing space is a dynamic property of the non-local BMP model and varies with W, i.e. the Turing space is related to the elasticity of the fluid.

The limit of small W reveals the nature and mechanism responsible for the length of the bands; these limits are

$$q_-^2 \sim \varphi_0, \quad q_+^2 \sim \frac{T}{D}, \tag{28}$$

and these relations indicate that the characteristic length of the bands is smaller than the length associated to the structure at a low shear-rate $\varphi_0^{-\frac{1}{2}}$ but larger than the length associated to the structural reformation time $T^{-\frac{1}{2}}$.

A. Eigenvalues of the Laplacian operator

The existence of the Turing space is a necessary, but not sufficient, condition for the existence of spatial instabilities. A sufficient condition includes the analysis of the Laplacian operator (Ponce, 2013). The eigenvalues of the Laplacian operator are solutions to the following eigenvalue equation:

$$\nabla^2 \boldsymbol{u} = -\lambda_D \boldsymbol{u}, \tag{29}$$

where λ_D is the eigenvalue related to the wavelength along which spatial terms grow. To provide a solution for Eq. (29), spatial patterns require periodic boundary conditions. A natural form to include periodic boundary conditions requires the concept of a cell of fluid of length L, with boundary conditions:

$$\boldsymbol{u}(t,0) = \boldsymbol{u}(t,L). \tag{30}$$

It can be shown that the solution to Eq. (29) is a combination of sine and cosine functions (the spectral representation of the Laplacian operator), that is, $\boldsymbol{u} = A\sin(\sqrt{\lambda_D}y) + B\cos(\sqrt{\lambda_D}y)$ (Ponce, 2013). With the boundary conditions (30), the following eigenvalues are obtained:

$$\lambda_D = \left(2\pi\frac{n}{L}\right)^2, \tag{31}$$

where $n = 1, 2, 3, \ldots$ represents the number of bands present in a cell of length L. The last condition for pattern formation requires that at least one eigenvalue λ_D exists inside the Turing space. Furthermore, it can be proved that $\lambda_D = q^2$; this result shows the connection between the boundary conditions [Eq. (30)], the geometry of the cell [Eq. (31)], and the possible length of the bands [Eq. (27)].

It is important to note that the Turing space is a dynamic property of the non-local BMP model [see Eq. (27)] and serves as a bound to the possible pattern lengths. While the eigenvalue λ_D does not depend on the parameters of the constitutive model in question, but on the geometry of the cell and the boundary conditions imposed [see Eq. (31)], it does define the actual length of the patterns allowed by the geometric arrangement of the cell. Hence, a sufficient condition requires that the length of the pattern allowed by the flow arrangement to be found within the possible lengths defined by the parameters of the fluid, i.e., $q_-^2 < \lambda_D < q_+^2$ (see Fig. 4 and Appendix B), a feedback between the characteristic lengths of the fluid and that of the flow arrangement. Such feedback has not been explicitly presented elsewhere, in the context of rheological complex fluids.

IV. AMPLITUDE FORMALISM

In Sec. III, a linearized version of the non-local BMP model is presented, and the conditions for the formation of spatial patterns are obtained (the critical point, related to the onset for banded flow, and patterns length). In this section, the contributions of non-linear terms are considered and the conditions for secondary instabilities are obtained.

A classical treatment for including non-linear contributions in dissipative structures consists of a perturbation expansion of the linear solution, to obtain the amplitude equations which describe temporal and spatial variations of the spatial patterns (Hohenberg and Halperin, 1977; Cross and Hohenberg, 1993; van Beijeren and Ernst, 1994; Cross and Greenside, 2009; and Wesfreid *et al.*, 1987). Amplitude equations are considered generic because they do not depend on the specific constitutive model considered, but on the dynamics of linear instability. Such equations can be used to describe qualitatively secondary instabilities (Manneville, 1990; Peña Pellicer, 2002; Cross and Hohenberg, 1993; and van Beijeren and Ernst, 1994).

Above the critical point q_c, there is a set of unstable waves given by (Manneville, 1990; Peña Pellicer, 2002; Cross and Hohenberg, 1993; and van Beijeren and Ernst, 1994):

$$\boldsymbol{u} = \int_{q\in\Delta q} \boldsymbol{u}(q)e^{iqy}dq = \int_{q\in\Delta q} \boldsymbol{u}_0 e^{\omega t}e^{i(q-q_c)y}e^{iq_c y}dq. \quad (32)$$

Here, $\boldsymbol{u}_0$ is the eigenvector corresponding to the critical point, and Δq is the set of wave numbers q within the Turing space [Eq. (26)]. Since ω represents the growth rate at the critical point and depends on both W and q, it can be expanded around W_c and q_c as:

$$\omega(W,q) \approx \omega_0[\mu - \xi_0^2(q-q_c)^2], \quad (33)$$

where ω_0, μ, and ξ are the growth rate close to the critical point, the normalized difference to the critical point, and the characteristic length corresponding to a wave number q, respectively. From the expansion of ω, it can be shown that:

$$\omega_0 = W_c\frac{\partial\omega}{\partial W}, \quad (34)$$

$$\mu = \frac{W-W_c}{W_c}, \quad (35)$$

$$-\xi_0^2 = \frac{1}{2W_c}\frac{1}{\partial\omega/\partial W}\frac{\partial^2\omega}{\partial q^2}. \quad (36)$$

Equation (33) shows that the linear relation for the temporal and the spatial variations of the envelope A has the form (van Beijeren and Ernst, 1994):

$$\frac{1}{\omega_0}\frac{\partial A(t,y)}{\partial t} = \mu A + \xi_0^2\frac{\partial^2 A(t,y)}{\partial y^2}. \quad (37)$$

In this equation, ξ_0 and ω_0 represent the characteristic length of the amplitudes and their characteristic rate, respectively. Also, this equation shows that the first temporal derivative of the amplitudes (the temporal scale) is proportional to the second spatial derivative (the square of the spatial scale), i.e., $\frac{\partial A(t,y)}{\partial t} \sim \frac{\partial^2 A(t,y)}{\partial y^2}$; such relation is useful for the derivation of the non-linear amplitude equation.

The method to obtain the non-linear amplitude equation consist of a perturbative expansion of the solution as a function of a small parameter (van Beijeren and Ernst, 1994). Such a procedure is presented in Appendix B, and the resulting non-linear amplitude equation is:

$$\frac{\partial A}{\partial t} = \frac{\partial^2 A}{\partial y^2} + \mu A - |A|^2 A. \quad (38)$$

In this equation, A can be, in general, a complex number, so the product in the cubic term yields an absolute square. Also the coefficients have been scaled out; only μ is kept explicit since it represents the difference with the critical value, W_c, and may be used as a parameter to describe secondary instabilities.

When $\mu < 0$ in Eq. (38), the only possible solution is $A = 0$; this solution represents a uniform system stable to spatial perturbations. On the other hand, when $\mu > 0$, Eq. (38) has stationary solutions of the form $A = A_0 e^{idqx}$ with $A_0^2 = \mu - dq^2$; these solutions describe stationary periodic patterns with wave numbers close to the critical value. Such scenario describes a supercritical bifurcation; note that the case of a subcritical bifurcation requires an amplitude equation of fifth order in A (Walgraef, 1996) and is not considered in this work.

The stability of the solutions depicted above follows from the Lyapunov function obtained from Eq. (38) (Manneville, 1990 and van Beijeren and Ernst, 1994), that is,

$$F = \int\left(\left|\frac{\partial A}{\partial y}\right|^2 - \mu|A|^2 + \frac{1}{2}|A|^4\right)dy, \quad (39)$$

from this expression follows that:

$$\frac{dF}{dt} = -2\int\left(\frac{\partial A}{\partial t}\right)^2 dy \le 0, \quad (40)$$

hence, the solutions to Eq. (38) are stable. Note that the first term inside the integral of Eq. (39) may be interpreted as a kinetic energy contribution, while the second and third terms may represent the potential energy corresponding to non-linear field. Therefore, when the equality holds on Eq. (40), the Lyapunov function represents the conservation of energy theorem for a conservative system (Manneville, 1990 and van Beijeren and Ernst, 1994).

In order to study the behavior of the spatial patterns in two dimensions, Eq. (38) has to be modified to include a second spatial variation. Note that transversal and longitudinal variations are qualitatively different. For this reason, a wave vector is considered as follows (van Beijeren and Ernst, 1994):

$$\boldsymbol{q} = \begin{pmatrix} \varepsilon^{\frac{1}{2}}q_x \\ q_c + \varepsilon q_y \end{pmatrix}. \quad (41)$$

Here, the difference in scaling along the two spatial directions reflects the breaking of rotational symmetry of the instability. The first order contributions come from the norm of the wave vector:

$$\nabla^2 \sim |\boldsymbol{q}|^2 - q_c^2 = (2q_c q_y + q_x^2)\varepsilon. \quad (42)$$

This equation represents the order relation of the wave numbers corresponding to different spatial directions, i.e. $q_y \sim q_x^2$; since the solutions were assumed as plain waves, the spatial variations follow a relation $2iq_c\frac{\partial}{\partial y} \sim \frac{\partial^2}{\partial x^2}$, and the two dimensional version of Eq. (38) is:

$$\frac{\partial A}{\partial t} = \left(\frac{\partial}{\partial y} - \frac{i}{2q_c}\frac{\partial^2}{\partial x^2}\right)^2 A + \mu A - |A|^2 A. \quad (43)$$

The stability of the solutions of Eq. (43) comes from a Lyapunov function analogous to that in Eq. (39); for this reason, the stability of Eq. (43) follows from the stability of Eq. (38) (Manneville, 1990 and van Beijeren and Ernst, 1994).

A. Phase equations

Non-linear solutions of the amplitude equations (38) and (43) may display modulations in magnitude and in phase (Manneville, 1990 and van Beijeren and Ernst, 1994). In order to discern between both of these contributions, an amplitude $A = |A|e^{i\phi}$ is proposed as a solution, first to Eq. (38), where real and imaginary terms are separated, to get:

$$\frac{\partial\phi}{\partial t} = \frac{\partial^2\phi}{\partial y^2} + \frac{2}{|A|}\frac{\partial|A|}{\partial y}\frac{\partial\phi}{\partial y}, \quad (44)$$

$$\frac{\partial|A|}{\partial t} = \frac{\partial^2|A|}{\partial y^2} + \left[\mu - \left(\frac{\partial\phi}{\partial y}\right)^2\right]|A| - |A|^3. \quad (45)$$

Here, the first term on the right-hand side of Eq. (44) shows that the phase evolution is primarily diffusive; this result agrees with experimental observations of shear bands (Fardin *et al.*, 2010; Fardin and Lerouge, 2012; and Lerouge *et al.*, 2008). On the other hand, Eq. (45) shows that the magnitude of the amplitudes is controlled by two contributions, occurring even in the absence of spatial variations; one of such contributions is related to μ, while the other comes from non-linear interactions.

For the phase equation corresponding to Eq. (43), a small perturbation on the amplitude A_0, corresponding to the one-dimensional periodic solution with wave number $dq = q - q_c$, is considered as follows (Manneville, 1990):

$$A(y) = (A_0 + a)e^{i(qy+\phi)}. \tag{46}$$

Substituting this expression into Eq. (43), and separating real and imaginary parts, the following linear equations are obtained:

$$\frac{\partial a}{\partial t} = -2A_0\left(A_0 a + dq\frac{\partial \phi}{\partial y}\right) + \frac{\partial^2 a}{\partial y^2} + \frac{dq}{q_c}\frac{\partial^2 a}{\partial x^2} + \frac{A_0}{q_c}\frac{\partial^3 \phi}{\partial y \partial x^2} - \frac{1}{4q_c^2}\frac{\partial^4 a}{\partial x^4}, \tag{47}$$

$$A_0\frac{\partial \phi}{\partial t} = 2dq\frac{\partial a}{\partial y} + A_0\frac{\partial^2 \phi}{\partial y^2} - \frac{1}{q_c}\frac{\partial^3 a}{\partial y \partial x^2} + A_0\frac{dq}{q_c}\frac{\partial^2 \phi}{\partial x^2} + \frac{A_0}{4q_c^2}\frac{\partial^4 \phi}{\partial x^4}. \tag{48}$$

According to Eq. (45), A relaxes slowly close to the critical point, while ϕ never relaxes because it represents a phase displacement. So, Eq. (47) may be simplified to its steady-state with higher order variations neglected (Manneville, 1990 and Peña Pellicer, 2002),

$$0 = A_0 a + dq\frac{\partial \phi}{\partial y}. \tag{49}$$

Additionally, phase evolution is primarily diffusive [see Eq. (44)], hence, in Eq. (48) higher order terms are neglected to obtain (Manneville, 1990 and Peña Pellicer, 2002):

$$\frac{\partial \phi}{\partial t} = \frac{2dq}{a_0}\frac{\partial a}{\partial y} + \frac{\partial^2 \phi}{\partial y^2} + \frac{dq}{q_c}\frac{\partial^2 \phi}{\partial x^2}. \tag{50}$$

These last two equations are combined to obtain the following two-dimensional phase equation (Manneville, 1990; van Beijeren and Ernst, 1994; and Peña Pellicer, 2002):

$$\frac{\partial \phi}{\partial t} = \left(\frac{\mu - 3dq^2}{\mu - dq^2}\right)\frac{\partial^2 \phi}{\partial y^2} + \frac{dq}{q_c}\frac{\partial^2 \phi}{\partial x^2}. \tag{51}$$

From this equation, the curves corresponding to primary marginal stability and secondary instabilities arise when the coefficients become negative (Manneville, 1990 and van Beijeren and Ernst, 1994). Such description is adequate for wave numbers close to the critical value q_c, but for the wave numbers farther away from q_c, higher-order terms in Eq. (51) are required (van Beijeren and Ernst, 1994).

V. RESULTS AND DISCUSSION

In Sec. III, the conditions for the formation of spatial patterns according to the non-local BMP model were given, and in this section the results of such conditions are presented using representative values inspired from experimental data. The numerical algorithm used is a separation of operators method with uniform mesh, where the initial conditions are the equilibrium solutions calculated from Eqs. (18) and (19), with a random spatial perturbation along the eigenvalue of the Laplacian operator, given by Eq. (31).

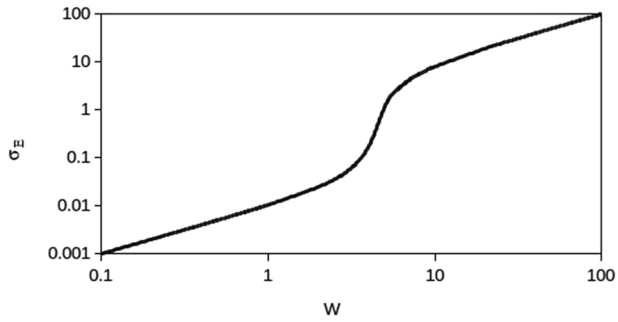

FIG. 1. Non-dimensional shear-stress as a function of the Weissenberg number for a shear-thickening fluid.

A. Homogeneous flow

As mentioned, spatial patterns are only possible for shear-thickening fluids when a cooperative interacting term is added in the constitutive model. The homogeneous steady-state solutions for the stress and the fluidity are plotted in Figs. 1 and 2, respectively; the parameters used in this section are $\varphi_0 = 100$, $K = 1$, $T = 0.2$, and $D = 2$. According to the BMP references (Bautista *et al.*, 1999; 2002; 2007; García-Sandoval *et al.*, 2012; and Manero *et al.*, 2007), the values of K and T are known to have a difference of $\mathcal{O}(2)$, the value of φ_0 is meant to represent a middle point between the continuous and discontinuous shear-thickening of micellar solutions (Townsend and Wilson, 2017 and Vázquez-Quesada *et al.*, 2017), and the value of D indicates that the mobilities of the shear-stress and fluidity are different but of the same order ($D_0 = \mathcal{O}(D_1)$).

Figure 1 depicts the growth of the steady-state shear-stress σ_E with the Weissenberg number W, in which a monotonic increase is predicted, i.e. there is no stress plateau. Figure 2 shows predictions from Eq. (19), illustrating a monotonic decrease of the fluidity with W. This is an example of the behavior of one stable phase within a homogeneous flow regime. Moreover, these solutions are locally stable against any homogeneous perturbation since conditions (23) and (24) are

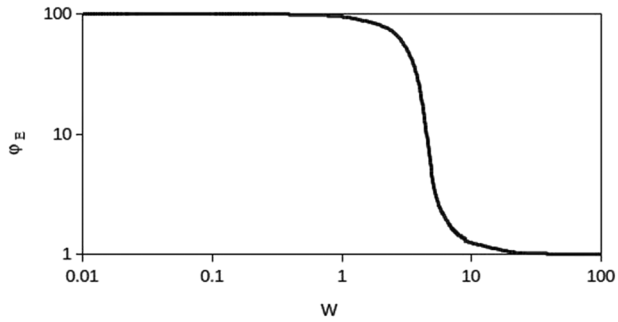

FIG. 2. Non-dimensional fluidity as function of the Weissenberg number for a shear-thickening-fluid.

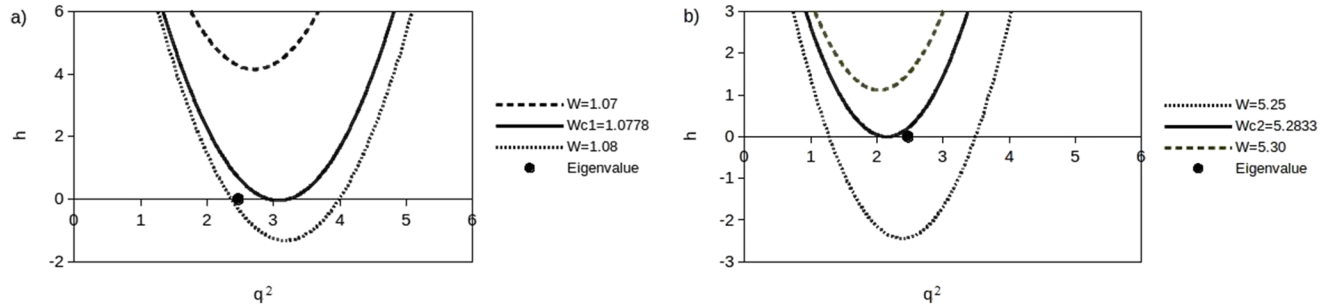

FIG. 3. $h(q^2)$ versus q^2 for different W values. (a) The upper curve ($W = 1.07$) presents no roots for $h(q^2)$ and hence no Turing space. The minimum of the curve with $W = 1.0778$ (first critical point) reaches zero. The lower curve ($W = 1.08$) presents two roots that determine the Turing space. The black circle represents the eigenvalue of the Laplacian operator. (b) The upper curve ($W = 5.30$) presents no roots for $h(q^2)$ and hence no Turing space. The minimum of the curve with $W = 5.2833$ (second critical point) reaches zero. The lower curve ($W = 5.25$) presents two roots that determine the Turing space. The black circle represents the eigenvalue of the Laplacian operator (the actual length of the patterns).

trivially fulfilled. The stability of the homogeneous solutions persist in the cubic BMP model because conditions (23) and (24) do not depend on the expansion of K as a function of $\dot{\gamma}$, i.e., the BMP model produces stable homogeneous solutions, even when a non-monotonic relation between shear-stress and shear-rate holds.

B. Stable spatial patterns

When the non-local terms set in, Fig. 3 displays solutions of $h(q^2)$ for different values of W. In Fig. 3(a), the curve corresponding to $W = 1.07$, and the minimum of $h(q^2)$ is always positive, as for the curve for $W = 5.30$ in Fig. 3(b); according to condition (26), for both these cases the homogeneous flow-regime is stable even against spatial perturbations. The curves corresponding to $W_{c1} = 1.0778$ in Fig. 3(a) and to $W_{c2} = 5.2833$ in Fig. 3(b) represent the critical points, wherein the minimum of the curves reaches zero; in these cases, the homogeneous solution is stable but perturbations around q_c may lead to unstable flow-regimes. Finally, the curves corresponding to $W = 1.08$ in Fig. 3(a) and to $W = 5.25$ in Fig. 3(b) present two roots, namely, q_-^2 and q_+^2. These values determine the intervals where the minimum of $h(q^2)$ is negative; along these intervals condition (26) is fulfilled, i.e., they determine the boundaries of the Turing space for each value of W. In these cases, the stable homogeneous system is unstable to any spatial perturbation and the fluid evolves into different phases, thereby conforming stable spatial patterns, i.e., dissipative structures.

Another condition for pattern formation is the existence of an eigenvalue of the diffusion operator in the Turing space. In Fig. 3, such eigenvalue is marked by a black circle. In this case, the ratio $\frac{n}{L}$ in Eq. (31) has a value of $\frac{1}{4}$, which means that the characteristic length of the bands is 4 times the characteristic length of the shear-stress; if the cell considered has an extension equal to or lower than 4, the fluid would lack space to form multiple bands, thereby the flow in this case becomes homogeneous. On the other hand, if the length of the cell is $4n$ with $n = 2, 3, 4, \ldots$ the fluid would have sufficient space to form n bands and the flow becomes inhomogeneous.

Furthermore, it should be noted that both, the minimum of $h(q^2)$ and the Turing space, vary with the W as predicted by Eqs. (26) and (27), while the black circle on Fig. 3, representing the eigenvalue of the Laplacian operator, is independent of the W, according to Eq. (31). Figure 3 also shows that critical point and the Turing space are moved around the eigenvalue of the Laplacian operator as W varies between W_{c1} and W_{c2}. In Fig. 4, the dependence of the critical point and of the Turing space on W is presented. The constant line represent the eigenvalue of the Laplacian operator that, in agreement with Eq. (31), is independent of W since it represents the length allowed by the flow arrangement. The continuous line represents the critical point q_c, and the two dashed lines represent the boundaries of the Turing space. These three lines, according to Eqs. (26) and (27), are functions of W and coincide with the bifurcation points, i.e., the beginning and the end of the banded states, representing the possible lengths of the spatial patterns defined by the fluid. Note that the relation of the critical curve with the eigenvalue of the Laplacian operator varies with W. This relation determines the difference between the fastest unstable mode ($\omega(q_c)$) and the growth rate of the actual pattern ($\omega(q)$); such difference may cause secondary instabilities.

Also, since the model includes non-local terms in the form of Laplacian operators, its eigenvalue always exists; but, for the fluid to form spatial patterns, the eigenvalue of the Laplacian operator must lie inside the Turing space (see Fig. 4). It is only for these values of W that the flow-regime may form banded states; so, in this scenario, the eigenvalue of the Laplacian operator plays the role of the shear-stress plateau, but the points where it enters and leaves the Turing space are related to the specific banded state and its stability rather than to the mechanical properties of the bands.

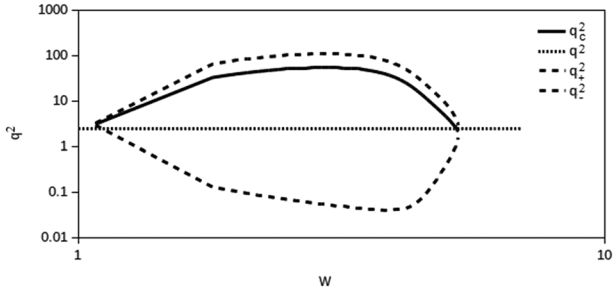

FIG. 4. Critical point and Turing space as a function of W. The constant line represents the eigenvalue of the Laplacian operator; this line is independent of W. The continuous line represents the critical wave number q_c and the two discontinuous lines represent the boundaries of the Turing space and how they vary with W.

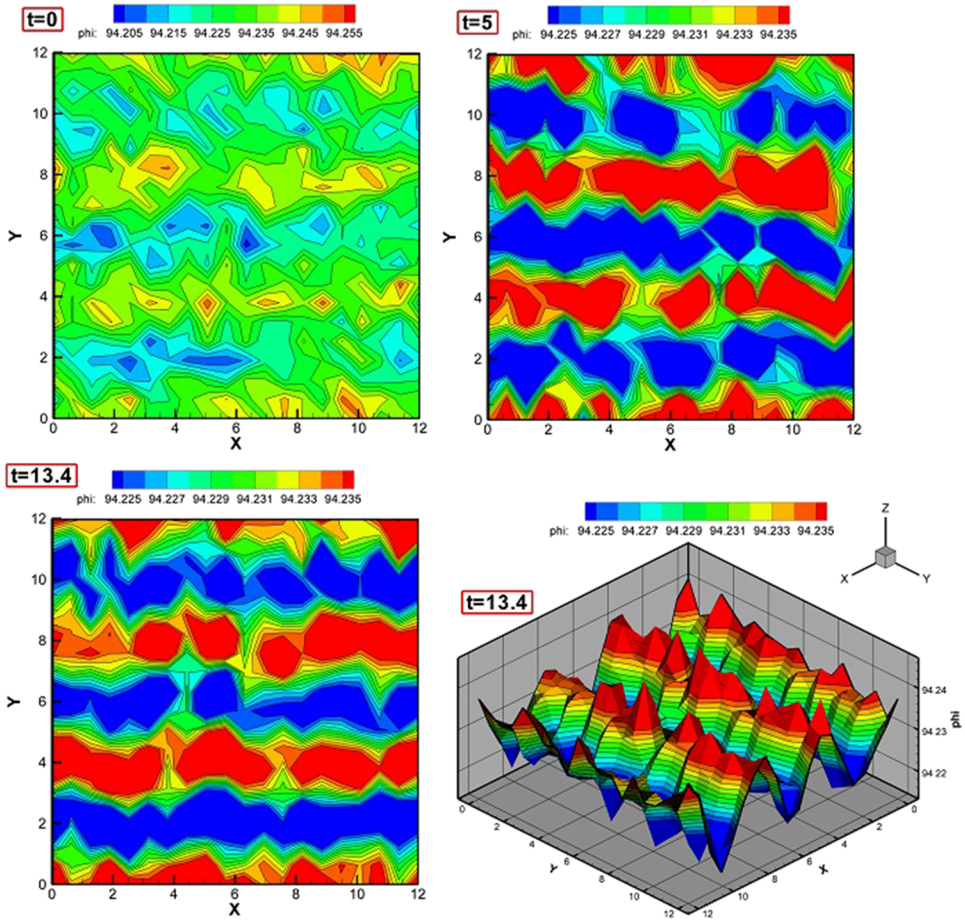

FIG. 5. Pattern formation in the nonlocal BMP model for shear-thickening fluids in the fluidity (structure variable). For $t = 0$, the initial conditions with a random spatial perturbation are shown. The patterns after five viscoelastic times ($t = 5$) reveal the pattern spatial evolution. After $t = 13.4$, the resulting spatial patterns resemble spatial bands with different fluidities.

The results of the simulations carried out with the nonlocal BMP model are shown in Figs. 5 and 6. The initial conditions at $t = 0$ correspond to the steady-state solution for the fluidity and the shear-stress [Eqs. (19) and (18), respectively] when a random spatial perturbation is applied along the direction of the eigenvalue of the operator [Eq. (31)]. The solutions evolve into semi-stable patterns for times $t = 5$, and for $t = 13.4$, the resulting spatial-patterns comprise a set of bands with different mechanical properties resembling shear bands.

One may note that in the final stable patterns, the amplitude of variations does not decrease to allow the fluid to recover its spatial homogeneity; rather, the fluid keeps the spatial patterns with the same amplitude at $t = 13.4$, indicating clearly that the inhomogeneous flow-regime is stable. According to condition (26), the term related to cooperative interaction of the structure is essential for the existence of the Turing space. Moreover, neglecting this term causes that the homogeneous state predicted by Eqs. (18) and (19) is recovered and it remains stable against local spatial perturbations.

For a shear-thickening fluid, the 3D plot in Fig. 5 reveals a phase with low fluidity (blue bands) and a phase with high fluidity (red bands). The 3D plot in Fig. 6 shows that the low fluidity phase supports a high stress concentration (red bands), while the high fluidity phase supports a low stress concentration (blue bands). Since the fluidity is related to the structural arrangement of the fluid itself (recall that the structure parameter is related to the micellar length n), one can see that, for low stress concentration, the fluid has a non-interactive, free structure that allows high mobility. On the other hand, for high stress concentration, the fluid has a highly interactive, entangled structure with low mobility. Hence, the bands formed have different mechanical properties.

C. Unstable spatial patterns

For wave numbers different to the critical value q_c, the pattern formation mechanism may not be as effective and secondary instabilities may arise. In a two-dimensional frame, instabilities may be parallel or perpendicular to the primary patterns shown in Fig. 5, as described by the amplitude equation (43). On the other hand, since secondary instabilities are mainly due to phase modulations, the phase equation (51) is a more natural way to describe stability curves, as shown in Fig. 7.

The primary instability curve, defining the beginning of the banded state, comes from values of dq and μ which cancel the denominator of the coefficient in the first term on the right-hand side of Eq. (51) (i.e., $\mu = dq^2$, see Fig. 7). For points below this curve, the pattern formation mechanism does not set in and the fluid presents only one stable phase. Additionally, the numerator of the same coefficient describes longitudinal instabilities (Eckhaus) that may appear when it changes sign and becomes negative. Equation (51) shows that the wave number causing this secondary instability is parallel to the primary instability shown in Fig. 5. For Eckhaus instabilities,

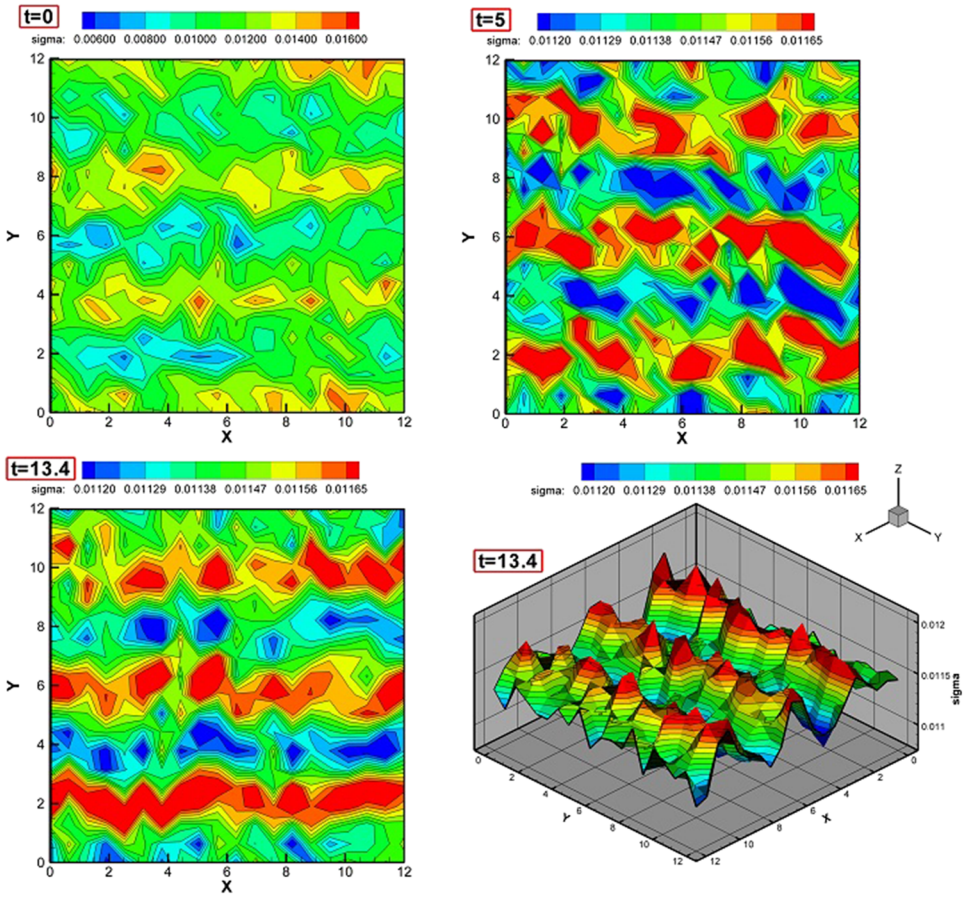

FIG. 6. Pattern formation in the non-local BMP model for shear-thickening fluids in the shear-stress. For $t = 0$, the initial conditions with a random spatial perturbation are shown. The patterns after five viscoelastic times ($t = 5$) reveal the pattern spatial evolution. After $t = 13.4$, the resulting spatial patterns resemble spatial bands supporting different shear-stresses.

the marginal curve is $\mu = 3dq^2$ (see Fig. 7). Points between the primary stability curve and the Eckhaus curve are close to the boundaries of the Turing space and, depending on the sing of dq, the wave vector is either too small or too large relative to its critical value q_c; hence, the patterns shown in Fig. 5 are unstable and bands may split or merge.

Transversal secondary instabilities (zig-zag) arise when the coefficient of the second term on the right-hand side of Eq. (51) changes sign and becomes negative. For zig-zag instabilities, the marginal curve is $dq = 0$ (see Fig. 7). Points on the right of the zig-zag curve ($dq > 0$) form stable banded states with wavelength close to q_c. While, for points on the left of the zig-zag curve ($dq < 0$), Eq. (51) shows that the wave number causing the secondary instability is perpendicular to the critical wave number of the primary instability shown in Fig. 5

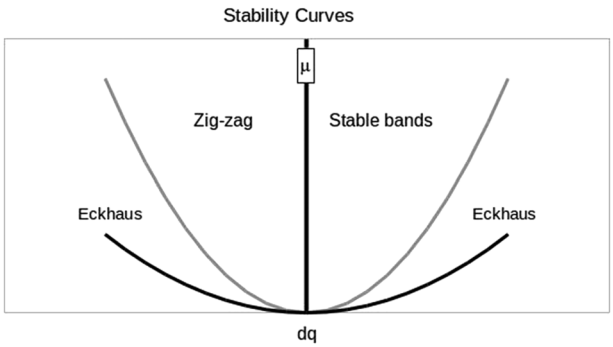

FIG. 7. Stability curves for the spatial patterns of the non-local BMP model.

and, since dq is small, both directions have similar wavelength; hence, the patterns at q_c are transversally unstable and present torsions with a wave number associated to dq.

These instabilities have been observed in experimental settings with *CPCI*/NaSal/*brine* and *CTAB*/$NaNO_3$ solutions with different visualization techniques such as light scattering, ultrasonic imaging, and birefringence.

In Fardin *et al.* (2010), they report a monotonic growth between shear-stress and shear-rate for the *CTAB*/$NaNO_3$ solution (see their Fig. 1). Such relation is also reported by Fardin *et al.* (2015) (see their Fig. 3), and by Lerouge *et al.* (2008) (see their Fig. 12). This monotonic growth agrees with the description presented in Fig. 1, which is contrary to the description of a stress-plateau (a zone of constant shear-stress for different values of shear-rate).

In contrast with experimental observations reported by Fardin and Lerouge (2012), the stress-plateau mechanism depicts a scenario where bands appear spontaneously. Fardin and Lerouge (2012) present PIV results of a *CTAB*/$NaNO_3$ solution (see their Fig. 4), where for small times, phase formation due to a diffusive-like mechanism is observed. Such results have also been reported by Lerouge *et al.* (2008) (see their Fig. 7). The phase formation reported there agrees with Eqs. (44) and (51), where phase modulations arise primarily due to diffusion.

Divoux *et al.* (2016) reported the results of ultrasonic imaging of a *CTAB*/$NaNO_3$ solution in which two bands with spatial undulations appear [see their Fig. 2(a)]. Similar results have also been reported by Fardin *et al.* (2010) (see their

Fig. 1), by Fardin *et al.* (2015) (see their Fig. 3), by Fardin and Lerouge (2012) (see their Figs. 4, 8, and 9), and by Lerouge *et al.* (2008) (see their Figs. 7 and 13). In the context of the present work, such behavior are manifestations of zig-zag instabilities that arise from a wave number close but lower than the critical wave number of the fluid, and which acts in a perpendicular direction to the critical wave number, as illustrated in Eq. (51) and in Fig. 7. Such an undulation of the interface cannot be predicted in the stress-plateau scenario without including stress-diffusion.

Multiple bands have already been reported within the stress-plateau approach, but they require a stress-diffusion term; when such term is neglected, only two stable bands are predicted. In Fardin *et al.* (2015), Fig. 5(b) display multiple spatial bands which remain stable; similar results have also been reported by Lerouge *et al.* (2008) in their Fig. 11(c). In the context of the present work, these bands are the stable dissipative structures shown in Fig. 5. Such structures arise from the Turing mechanism and require a wave number greater but close to q_c, as shown in Fig. 7.

In Lerouge *et al.* (2008) Figs. 11(b) and 11(d), the number of bands and their length are different to those bands in Fig. 11(c). These results are manifestations of Eckhaus instabilities, where the wave number is close to the boundaries of the Turing space, and bands may split or merge in order to adjust their length to the wave number defined by the Laplacian operator instead of the critical wave number.

These dynamic results are contrary to the stress-plateau paradigm, for which no shear-stress diffusion is considered, since it neglects the spatial variations of shear-stress and fluidity. In the present work it has been proven that the stress-plateau has no effect on the spatial stability of the fluid, and that different phases with dynamic behaviors arise from spatial variations of shear-stress and fluidity alone.

VI. CONCLUSIONS

Shear-banding is a phenomenon commonly ascribed to a mechanical instability or spinodal decomposition related to the existence of a stress-plateau. In this work, it was demonstrated that complex fluids with a monotonic relation between the shear-stress and the shear-rate may induce spatial patterns (dissipative structures) that resemble shear bands, if cooperative interactions and mobilities of a structural variable (fluidity) and shear-stress are included in the constitutive equation.

It was shown that the extension of the Turing space is determined by the constitutive equations, as shown in Eq. (27). The Turing space bounds the possible lengths of the patterns but does not define the actual length observed. The length of the bands is related to the boundary conditions and to the extension of the flow cell through the Laplacian operator, as shown in Eq. (31).

Shear-thickening fluids allow the definition of a critical point for an instability of Turing-type. In this case, the Turing space is well-defined, with bounded characteristic lengths. The Turing mechanism presented here allows the formation of multiple bands without the presence of a stress-plateau. Hence, fluids with monotonic flow-curves can evolve into banded states. In the present work, it is proven that the stress-plateau has no effect on the stability, and that different phases with dynamic behaviors arise from spatial variations of shear-stress and fluidity exclusively.

An important conclusion is that the cross-spatial term in the constitutive model is a necessary condition for the formation of dissipative structures. In addition, spatial patterns may be more dynamic than the classical shear bands as shown in the simulations. They can support further instabilities causing band torsion and/or band nucleation, as the amplitude formalism demonstrates. Such secondary instabilities have been extensively reported in the literature and, through the phase equation, qualitative comparisons may be drawn.

The present work deals only with spatial instabilities in shear-thickening fluids. Shear-thinning fluids and spatio-temporal instabilities remain untreated and are under consideration in a forthcoming publication.

ACKNOWLEDGMENTS

M. Turcio gratefully acknowledges the financial support from Project No. CB2014-235880 from CONACYT (Consejo Nacional de Ciencia y Tecnología) and a Ph.D. grant also from CONACYT.

A. Capella gratefully acknowledges the financial support from Grant No. PAPIIT IN106118 by DGAPA UNAM 397.

J. E. López-Aguilar gratefully acknowledges the financial support from PAIP (5000-9172, FQ UNAM, México), PAPIIT (IA105818, UNAM, México), and CONACYT.

APPENDIX A: GENERALIZED BMP MODEL

Equations (5) and (4) arise from an extended thermodynamic description of complex fluids, wherein a scalar (the fluidity φ), a vector (the diffusive current $\boldsymbol{J}$), and a tensor (the stress $\boldsymbol{\sigma}$) are the fast variables of the respective relaxation equations (Manero *et al.*, 2007). For simple-shear (where x is the direction of the macroscopic flow velocity, y is the direction of the velocity-gradient and z is the vorticity direction), we assume the following conditions: (a) small inertia, (b) negligible concentration gradients, (c) the mass flux relaxation time is negligible small compared to the stress relaxation time ($\frac{1}{G\varphi} \gg \tau_1$), and (d) translational symmetry of the flow: the particular case where the derivatives in the direction of flow are negligible, (e) constant phenomenological parameters. In such case, Eqs. (5) and (4) become:

$$\frac{d\varphi}{dt} = \frac{\varphi_0 - \varphi}{T} + k(\varphi_\infty - \varphi)\sigma_{xy}\dot{\gamma} + \beta_0' \frac{\partial J_y}{\partial y}, \tag{A1}$$

$$J_x = \pm\beta_2 \frac{\partial \sigma_{xy}}{\partial y}, \tag{A2}$$

$$J_y = \beta_0 \frac{\partial \varphi}{\partial y} \pm \beta_2 \frac{\partial \sigma_{yy}}{\partial y}, \tag{A3}$$

$$\sigma_{xy} + \frac{1}{G\varphi}\left(\frac{\partial \sigma_{xy}}{\partial t} - \dot{\gamma}\sigma_{yy}\right) = \frac{\dot{\gamma}}{\varphi} + \frac{\beta_2'}{2}\frac{\partial J_x}{\partial y}, \tag{A4}$$

$$\sigma_{xx} + \frac{1}{G\varphi}\left(\frac{\partial \sigma_{xx}}{\partial t} - 2\dot{\gamma}\sigma_{xy}\right) = 0, \tag{A5}$$

$$\sigma_{yy} + \frac{1}{G\varphi}\frac{\partial \sigma_{yy}}{\partial t} = \beta_2'\left(\frac{\partial J_y}{\partial y}\right), \tag{A6}$$

$$\sigma_{zz} + \frac{1}{G\varphi}\frac{\partial \sigma_{zz}}{\partial t} = 0. \tag{A7}$$

From Eqs. (A2) and (A3), upon performing the derivatives and substitution into Eqs. (A1), (A4), and (A6) we obtain:

$$\frac{d\varphi}{dt} = \frac{\varphi_0 - \varphi}{T} + k(\varphi_\infty - \varphi)\sigma_{xy}\dot{\gamma} + \beta_0'\beta_0\frac{\partial^2\varphi}{\partial y^2} \pm \beta_0'\beta_2\frac{\partial^2\sigma_{yy}}{\partial y^2}, \tag{A8}$$

$$\sigma_{xy} + \frac{1}{G\varphi}\left(\frac{\partial \sigma_{xy}}{\partial t} - \dot{\gamma}\sigma_{yy}\right) = \frac{\dot{\gamma}}{\varphi} \pm \frac{\beta_2'\beta_2}{2}\frac{\partial^2\sigma_{xy}}{\partial y^2}, \tag{A9}$$

$$\sigma_{yy} + \frac{1}{G\varphi}\frac{\partial \sigma_{yy}}{\partial t} = \beta_2'\beta_0\frac{\partial^2\varphi}{\partial y^2} \pm \beta_2'\beta_2\frac{\partial^2\sigma_{yy}}{\partial y^2}. \tag{A10}$$

Next, the normal-stress differences are defined in the usual form:

$$N_1 = \sigma_{xx} - \sigma_{yy}, \quad N_2 = \sigma_{yy} - \sigma_{zz}. \tag{A11}$$

Hence, from Eqs. (A5)–(A7), the following equation for the normal stresses is obtained:

$$(N_1 + N_2) + \frac{1}{G\varphi}\left(\frac{\partial(N_1 + N_2)}{\partial t} - 2\dot{\gamma}\sigma_{xy}\right) = 0. \tag{A12}$$

As observed, Eq. (A12) is decoupled from the three equations (A8)–(A10). It is possible to analyze the stability of the system of Eqs. (A8)–(A10). However, a reduction to a two-variable system can be obtained by considering the following assumptions: (a) Eq. (A10) attains its steady-state faster than Eq. (A9) (quasi-steady-state assumption) such as the time derivative approaches zero. (b) The second derivative of the normal-stress σ_{yy} in Eqs. (A8) and (A10) is negligible. In such case we obtain:

$$\sigma_{yy} = \beta_2'\beta_0\frac{\partial^2\varphi}{\partial y^2}, \tag{A13}$$

which upon substitution into Eq. (A9) renders:

$$\sigma_{xy} + \frac{1}{G\varphi}\left(\frac{\partial \sigma_{xy}}{\partial t} - \dot{\gamma}\beta_2'\beta_0\frac{\partial^2\varphi}{\partial y^2}\right) = \frac{\dot{\gamma}}{\varphi} \pm \frac{\beta_2'\beta_2}{2}\frac{\partial^2\sigma_{xy}}{\partial y^2}, \tag{A14}$$

where the variable relaxation time is $\frac{1}{G\varphi}$. Equation (A14) together with Eq. (A15):

$$\frac{d\varphi}{dt} = \frac{\varphi_0 - \varphi}{T} + k(\varphi_\infty - \varphi)\sigma_{xy}\dot{\gamma} + \beta_0'\beta_0\frac{\partial^2\varphi}{\partial y^2}, \tag{A15}$$

are the two variable systems to be analyzed. Defining the structure spatial coefficient D_0, the stress spatial coefficient D_1 (multiplied by the relaxation time $\frac{1}{G\varphi}$), and the Weissenberg number W, respectively, as:

$$\begin{aligned} D_0(W) &= \beta_0'\beta_0 = \dot{\gamma}\beta_2'\beta_0, \\ D_1(W) &= G\varphi\frac{\beta_2'\beta_2}{2}, \\ W &= \frac{\dot{\gamma}}{G\varphi_\infty}. \end{aligned} \tag{A16}$$

The following set of equations is obtained:

$$\frac{\partial \sigma_{xy}}{\partial t} = -G\varphi\sigma_{xy} + \dot{\gamma}G + \frac{GD_0(W)}{\varphi_\infty}\nabla^2\varphi \pm D_1(W)\nabla^2\sigma_{xy}, \tag{A17}$$

$$\frac{\partial \varphi}{\partial t} = \frac{\varphi_0 - \varphi}{T} + k(\varphi_\infty - \varphi)\sigma_{xy}\dot{\gamma} + D_0(W)\nabla^2\varphi. \tag{A18}$$

The stability analysis considers only small departures from the critical Weissenberg (W_c); thus, as a further simplification, the spatial coefficients ($D_0(W)$ and $D_1(W)$) in Eqs. (A17) and (A18) can be considered constant around W_c leading to Eqs. (8) and (9).

APPENDIX B: DERIVATION OF THE NON-LINEAR AMPLITUDE EQUATION

The solution close to the critical point (W_c, q_c) may be expanded as a function of a small parameter, $\epsilon = W - W_c$, and the non-linear equation may be replaced by a system of linear equations at different orders of ϵ (Manneville, 1990; Peña Pellicer, 2002; and van Beijeren and Ernst, 1994) so that the linear operator in (22), together with the non-linear parts and the Weissenberg number, must be expanded as follows:

$$\boldsymbol{u} \approx \epsilon\boldsymbol{u}_1 + \epsilon^2\boldsymbol{u}_2 + \epsilon^3\boldsymbol{u}_3 + \cdots, \tag{B1}$$

$$\boldsymbol{l} \approx \boldsymbol{l}_0 + \epsilon\boldsymbol{l}_1 + \epsilon^2\boldsymbol{l}_2 + \cdots, \tag{B2}$$

$$\boldsymbol{N} \approx \epsilon^2\boldsymbol{N}_2 + \epsilon^3\boldsymbol{N}_3 + \cdots, \tag{B3}$$

$$W \approx W_c + \epsilon W_1 + \epsilon^2 W_2 + \cdots. \tag{B4}$$

Note that the expansion of W causes that the equilibrium values, σ_E and φ_E, also change with ϵ; so these equilibrium values may be approximated as:

$$\begin{aligned} \sigma_E &\approx \sigma_E(W_c) + \epsilon\sigma_E(W_1) + \epsilon^2\sigma_E(W_2) + \cdots, \\ &\approx \sigma_{E0} + \epsilon\sigma_{E1} + \epsilon^2\sigma_{E2} + \cdots, \end{aligned} \tag{B5}$$

$$\begin{aligned} \varphi_E &\approx \varphi_E(W_c) + \epsilon\varphi_E(W_1) + \epsilon^2\varphi_E(W_2) + \cdots, \\ &\approx \varphi_{E0} + \epsilon\varphi_{E1} + \epsilon^2\varphi_{E2} + \cdots. \end{aligned} \tag{B6}$$

In these expressions, the terms σ_{Ej} and φ_{Ej} represent deviations from σ_E and φ_E, respectively, caused by W_j.

For the expansion of the differential operators, $\frac{\partial}{\partial t}$ and $\frac{\partial}{\partial y}$, the order relation obtained in the linear amplitude equation (37) is used (Manneville, 1990; Peña Pellicer, 2002; and van Beijeren and Ernst, 1994), so the proposed expansions are:

$$\frac{\partial}{\partial t} \approx \frac{\partial}{\partial t_0} + \epsilon^2\frac{\partial}{\partial t_1}, \tag{B7}$$

$$\frac{\partial}{\partial y} \approx \frac{\partial}{\partial y_0} + \epsilon\frac{\partial}{\partial y_1}. \tag{B8}$$

Upon substitution of the relations (B1)–(B8), and by arranging the result in different orders of ϵ, the following system is obtained:

$$\frac{\partial \boldsymbol{u}_1}{\partial t_0} = \boldsymbol{l}_0 \cdot \boldsymbol{u}_1, \tag{B9}$$

$$\frac{\partial \boldsymbol{u}_2}{\partial t_0} = \boldsymbol{l}_0 \cdot \boldsymbol{u}_2 + \boldsymbol{l}_1 \cdot \boldsymbol{u}_1 + \boldsymbol{N}_2, \tag{B10}$$

$$\frac{\partial \boldsymbol{u}_3}{\partial t_0} + \frac{\partial \boldsymbol{u}_1}{\partial t_1} = \boldsymbol{l}_0 \cdot \boldsymbol{u}_3 + \boldsymbol{l}_1 \cdot \boldsymbol{u}_2 + \boldsymbol{l}_2 \cdot \boldsymbol{u}_1 + \boldsymbol{N}_3, \tag{B11}$$

where:

$$\boldsymbol{l}_0 = \begin{pmatrix} -\varphi_{E0} + \frac{\partial^2}{\partial y_0^2} & -\sigma_{E0} + D\frac{\partial^2}{\partial y_0^2} \\ KW_c(1 - \varphi_{E0}) & -T - KW_c\sigma_{E0} + D\frac{\partial^2}{\partial y_0^2} \end{pmatrix}, \tag{B12}$$

$$\boldsymbol{l}_1 = \begin{pmatrix} -\varphi_{E1} + 2\frac{\partial^2}{\partial y_0 \partial y_1} & -\sigma_{E1} + 2D\frac{\partial^2}{\partial y_0 \partial y_1} \\ K(W_1 - W_c\varphi_{E1} - W_1\varphi_{E0}) & -K(W_c\sigma_{E1} + W_1\sigma_{E0}) + 2D\frac{\partial^2}{\partial y_0 \partial y_1} \end{pmatrix}, \tag{B13}$$

$$\boldsymbol{l}_2 = \begin{pmatrix} -\varphi_{E2} + \frac{\partial^2}{\partial y_1^2} & -\sigma_{E2} + D\frac{\partial^2}{\partial y_1^2} \\ K(W_2 - W_c\varphi_{E2} - W_1\varphi_{E1} - W_2\varphi_{E0}) & -K(W_c\sigma_{E2} + W_1\sigma_{E1} + W_2\sigma_{E0}) + D\frac{\partial^2}{\partial y_1^2} \end{pmatrix}, \tag{B14}$$

$$\boldsymbol{N}_2 = -\begin{pmatrix} 1 \\ KW_c \end{pmatrix}\hat{\sigma}_1\hat{\varphi}_1, \tag{B15}$$

$$\boldsymbol{N}_3 = -\begin{pmatrix} \hat{\sigma}_1\hat{\varphi}_2 + \hat{\sigma}_2\hat{\varphi}_1 \\ KW_c(\hat{\sigma}_1\hat{\varphi}_2 + \hat{\sigma}_2\hat{\varphi}_1) + KW_1\hat{\sigma}_1\hat{\varphi}_1 \end{pmatrix}. \tag{B16}$$

1. Order ϵ

Equation (B9) shows that, at order ϵ, the linear equation is recovered, and its solution is:

$$\boldsymbol{u}_1 = \boldsymbol{u}_0 e^{iq_c y}, \tag{B17}$$

where $\boldsymbol{u}_0$ represents the eigenvector of $\boldsymbol{l}_0$, that is,

$$\boldsymbol{u}_0 = \begin{pmatrix} 1 \\ \alpha \end{pmatrix} = \begin{pmatrix} 1 \\ \frac{KW_c(1-\varphi_{E0})}{T + KW_c\sigma_{E0} + Dq_c^2} \end{pmatrix}. \tag{B18}$$

For orders greater than ϵ, the resulting equations have the form $\left(\frac{\partial}{\partial t_0} - \boldsymbol{l}_0\right)\cdot \boldsymbol{u}_j = \underline{I}_j$. The operator on the left-hand side of these expressions is singular; hence, its solution has to be restricted to subspaces where it is invertible. Such subspaces are given by the Fredholm condition (Manneville, 1990; Peña Pellicer, 2002; and van Beijeren and Ernst, 1994):

$$\boldsymbol{v}_0 \cdot \underline{I}_j = 0, \tag{B19}$$

where $\boldsymbol{v}_0$ is the left eigenvector of $\boldsymbol{l}_0$, that is,

$$\boldsymbol{v}_0^T = \begin{pmatrix} 1 \\ \beta \end{pmatrix} = \begin{pmatrix} 1 \\ \frac{\varphi_{E0} + q_c^2}{KW_c(1-\varphi_{E0})} \end{pmatrix}. \tag{B20}$$

2. Order ϵ^2

At this order, the Fredholm condition leads to $\boldsymbol{v}_0 \cdot \boldsymbol{l}_1 \cdot \boldsymbol{u}_1 = 0$; then, real and imaginary parts of this expression are separated and cancelled to get:

$$\beta K(1 - \varphi_{E0} - \alpha\sigma_{E0})W_1^2 - (\varphi_{E1} + \alpha\sigma_{E1})(1 + \beta KW_c)W_1 = 0, \tag{B21}$$

$$2q_c(1 + \alpha D + \alpha\beta D)\frac{\partial W_1}{\partial y_1} = 0. \tag{B22}$$

Here, Eq. (B22) is trivially fulfilled because $1 + \alpha D + \alpha\beta D = 0$. On the other hand, Eq. (B21) requires that $W_1 = 0$. These results indicate that the normal form of the bifurcation is $\frac{\partial E}{\partial t} = \mu E - gE^3$. Also, since $W_1 = 0$, the expressions (B4)–(B6) and the operators (B13), (B14), and (B16) are simplified to:

$$\boldsymbol{l}_1 = \begin{pmatrix} 2\frac{\partial^2}{\partial y_0 \partial y_1} & +2D\frac{\partial^2}{\partial y_0 \partial y_1} \\ 0 & 2D\frac{\partial^2}{\partial y_0 \partial y_1} \end{pmatrix}, \tag{B23}$$

$$\boldsymbol{l}_2 = \begin{pmatrix} -\varphi_{E2} + \frac{\partial^2}{\partial y_1^2} & -\sigma_{E2} + D\frac{\partial^2}{\partial y_1^2} \\ K(W_2 - W_c\varphi_{E2} - W_2\varphi_{E0}) & -K(W_c\sigma_{E2} + W_2\sigma_{E0}) + D\frac{\partial^2}{\partial y_1^2} \end{pmatrix}, \tag{B24}$$

$$\boldsymbol{N}_3 = -\begin{pmatrix} 1 \\ KW_c \end{pmatrix}(\hat{\sigma}_1\hat{\varphi}_2 + \hat{\sigma}_2\hat{\varphi}_1). \tag{B25}$$

Finally, the solution $\boldsymbol{u}_2$ is the combination of the solution to the problem at order ϵ with resonant terms (Manneville, 1990; Peña Pellicer, 2002; and van Beijeren and Ernst, 1994):

$$\boldsymbol{u}_2 = \begin{pmatrix} 1 \\ \alpha \end{pmatrix} C_2 e^{iq_c y} + \begin{pmatrix} a_1 \\ b_1 \end{pmatrix} e^{iq_c y} + \begin{pmatrix} a_2 \\ b_2 \end{pmatrix} e^{2iq_c y}. \tag{B26}$$

Here, coefficients a_j and b_j $(j = 1, 2)$ are obtained upon substitution of the solution (B26) in Eq. (B10) (Peña Pellicer, 2002) so that:

$$a_1 - \frac{1}{\alpha}b_1 = 2iq_c\left(\frac{1 + \alpha D}{\varphi_{E0} + q_c^2}\right)\frac{\partial C_1}{\partial y_1}, \tag{B27}$$

$$a_2 = -\left(\frac{4Dq_c^2(1 - KW_c) + T}{8Dq_c^4 + T\varphi_{E0} + KW_c\sigma_{E0}}\right)\alpha C_1^2, \tag{B28}$$

$$b_2 = -\left(\frac{KW_c(4q_c^2 + 1)}{8Dq_c^4 + T\varphi_{E0} + KW_c\sigma_{E0}}\right)\alpha C_1^2. \tag{B29}$$

3. Order ϵ^3

Using the Fredholm condition (B19) on Eq. (B11) leads to:

$$\boldsymbol{v}_0 \cdot \frac{\partial \boldsymbol{u}_1}{\partial t_1} = \boldsymbol{v}_0 \cdot \boldsymbol{l}_1 \cdot \boldsymbol{u}_2 + \boldsymbol{v}_0 \cdot \boldsymbol{l}_2 \cdot \boldsymbol{u}_1 + \boldsymbol{v}_0 \cdot \boldsymbol{N}_3, \tag{B30}$$

for simplicity, this expression is analyzed separately. The left-hand side term is used to obtain:

$$\boldsymbol{v}_0 \cdot \frac{\partial \boldsymbol{u}_1}{\partial t_1} = (1 + \alpha\beta)\frac{\partial C_1}{\partial t_1}. \tag{B31}$$

The first term on the right-hand side of Eq. (B30) is:

$$\boldsymbol{v}_0 \cdot \boldsymbol{l}_1 \cdot \boldsymbol{u}_2 = -4q_c^2\left(\frac{1+\alpha D}{\varphi_{E0}+q_c^2}\right)\frac{\partial^2 C_1}{\partial y_1^2}, \tag{B32}$$

whilst the second term on the right-hand side of Eq. (B30) leads to:

$$\begin{aligned}\boldsymbol{v}_0 \cdot \boldsymbol{l}_2 \cdot \boldsymbol{u}_1 = [&\varphi_{E2} - \alpha\sigma_{E2} + K(W_2 - W_c\varphi_{E2} - W_2\varphi_{E0})\beta \\ &- K(W_c\sigma_{E2} + W_2\sigma_{E0})\alpha\beta]C_1.\end{aligned} \tag{B33}$$

The third term on the right-hand side of Eq. (B30) is used to get:

$$\boldsymbol{v}_0 \cdot \boldsymbol{N}_3 = \left(\frac{4q_c^2[KW_c(1-\alpha D)+\alpha D] + KW_c + \alpha T}{8Dq_c^4 + T\varphi_{E0} + KW_c\sigma_{E0}}\right)\alpha|C_1|^2C_1. \tag{B34}$$

Substituting terms (B31)–(B34) on Eq. (B30), and rearranging the resulting expression to get:

$$\frac{1}{\omega_0}\frac{\partial C_1}{\partial t_1} = \xi_0^2\frac{\partial^2 C_1}{\partial y_1^2} + \frac{W_2}{W_c}C_1 - g|C_1|^2C_1. \tag{B35}$$

When this expression is multiplied by ϵ^3, the original operators are recovered and the resulting non-linear amplitude equation is (Manneville, 1990; Peña Pellicer, 2002; and van Beijeren and Ernst, 1994):

$$\frac{1}{\omega_0}\frac{\partial A}{\partial t} = \xi_0^2\frac{\partial^2 A}{\partial y^2} + \mu A - g|A|^2A. \tag{B36}$$

Here, coefficients ω_0, ξ_0, and μ agree with those from the linear equation (37), and g may be obtained from the deduction of Eq. (B35). These parameters may be scaled out of the amplitude equation (38) (van Beijeren and Ernst, 1994).

Aradian, A. and Cates, M. E., "Instability and spatiotemporal rheochaos in a shear-thickening fluid model," Europhys. Lett. **70**(3), 397–403 (2005).

Bautista, F., de Santos, J. M., Puig, J. E., and Manero, O., "Understanding thixotropic and antithixotropic behavior of viscoelastic micellar solutions and liquid crystalline dispersions. I. The model," J. Non-Newtonian Fluid Mech. **80**, 93–113 (1999).

Bautista, F., Soltero, J. F., Macías, E. R., Puig, J. E., and Manero, O., "Irreversible thermodynamics approach and modeling of shear-banding flow of wormlike micelles," J. Phys. Chem., B **106**, 13018–13026 (2002).

Bautista, F., Pérez-López, J. H., García, J. P., Puig, J. E., and Manero, O., "Stability analysis of shear banding flow with the BMP model," J. Non-Newtonian Fluid Mech. **144**, 160–169 (2007).

Bhave, A. V., Armstrong, R. C., and Brown, R. A., "Kinetic theory and rheology of dilute, nonhomogeneous polymer solutions," J. Chem. Phys. **95**, 2988 (1991).

Cates, M. E., "Reptation of living polymers: dynamics of entangled polymers in the presence of reversible chain-scission reactions," Macromolecules **20**, 2289–2296 (1987).

Cates, M. E. and Fielding, S. M., "Rheology of giant micelles," Adv. Phys. **55**, 799–879 (2006).

Cross, M. C. and Greenside, H., *Pattern Formation and Dynamics in Nonequilibrium Systems* (Cambridge University Press, USA, 2009).

Cross, M. C. and Hohenberg, P. C., "Pattern formation outside of equilibrium," Rev. Mod. Phys. **65**, 851 (1993).

Divoux, T., Fardin, M. A., Manneville, S., and Lerouge, S., "Shear banding of complex fluids," Annu. Rev. Fluid Mech. **48**, 81–103 (2016).

Doi, M. and Edwards, S. F., *The Theory of Polymer Dynamics* (Clarendon Press, 1989).

El-Kareth, A. W. and Leal, L. G., "Existence of solutions for all Deborah numbers for a non-Newtonian model modified to include diffusion," J. Non-Newtonian Fluid Mech. **33**, 257–287 (1989).

Fardin, M. A. and Lerouge, S., "Instabilities in wormlike micelle systems," Eur. Phys. J. E **35**, 1–28 (2012).

Fardin, M. A., Lopez, D., Croso, J., Gregoire, G., Cardoso, O., McKinley, G. H., and Lerouge, S., "Elastic turbulence in shear banding wormlike micelles," Phys. Rev. Lett. **104**, 178303 (2010).

Fardin, M. A., Radulescu, O., Morozov, A., Cardoso, O., Browaeys, J., and Lerouge, S., "Stress diffusion in shear banding wormlike micelles," J. Rheol. **59**(6), 1335–1362 (2015).

Fielding, S. M. and Wilson, H. J., "Shear banding and interfacial instability in planar Poiseuille flow," J. Non-Newtonian Fluid Mech. **165**, 196–202 (2010).

Gambino, G., Lombardo, M. C., and Sammartino, M., "Turing instability and traveling fronts for a nonlinear reaction–diffusion system with cross-diffusion," Math. Comput. Simul. **82**, 1112–1132 (2012).

García-Sandoval, J. P., Manero, O., Bautista, F., and Puig, J. E., "Inhomogeneous flows and shear banding formation in micellar solutions: Predictions of the BMP model," J. Non-Newtonian Fluid Mech. **179-180**, 43–54 (2012).

Hohenberg, P. C. and Halperin, B. I., "Theory of dynamic critical phenomena," Rev. Mod. Phys. **49-3**, 435–479 (1977).

Kim, S. H. and Park, H. S., "Dissipative structures of autocatalytic reactions in tubular flow reactors," Korean J. Chem. Eng. **10**(4), 226–234 (1993).

Larson, R. G., "Instabilities in viscoelastic flows," Rheol. Acta **31**, 213–263 (1992).

Lerouge, S. and Berret, J.-F., "Shear-induced transitions and instabilities in surfactant wormlike micelles," in *Advances in Polymer Science*, Polymer Characterization Vol 230 (Springer, Berlin, Heidelberg, 2009).

Lerouge, S., Fardin, M. A., Argentina, M., Grégoirea, G., and Cardoso, O., "Interface dynamics in shear-banding flow of giant micelles," Soft Matter **9**, 1808 (2008).

Manero, O., Pérez-López, J. H., Escalante, J. I., Puig, J. E., and Bautista, F., "A thermodynamic approach to rheology of complex fluids: The generalized BMP model," J. Non-Newtonian Fluid Mech. **146**, 22–29 (2007).

Manneville, P., *Dissipative Structures and Weak Turbulence* (Academic Press, United Kingdom, 1990).

Manneville, S., "Recent experimental probes of shear banding," Rheol. Acta **47**, 301–318 (2008).

Mead, D. W., Larson, R. G., and Doi, M., "A molecular theory for fast flows of entangled polymers," Macromolecules **31**, 7895–7914 (1998).

Mitkin, V. V. and Thofanous, T. G., "The physics of aerobreakup. IV. Strain-thickening liquids," Phys. Fluids **29**, 122101 (2017).

Nicolis, G. and Prigogine, I., *Self-Organization in Nonequilibrium Systems* (Wiley-Interscience, USA, 1977).

Olmsted, P. D., "Perspectives on shear banding in complex fluids," Rheol. Acta **47**, 283–300 (2008).

Öttinger, H. C., "Incorporation of polymer diffusivity and migration into constitutive equations," Rheol. Acta **31**, 14–21 (1992).

Peña Pellicer, B., "Inestabilidades de Turing en sistemas de reacción difusión," Ph.D. dissertation (Navarra University, Spain, 2002).

Ponce, A. V., "Formación de patrones por el mecanismo de Turing en sistemas de reacción-difusión," Undergraduate dissertation (UNAM, México, 2013).

Porte, G., Berret, J. F., and Harden, J. L., "Inhomogeneous flows of complex fluids: Mechanical instability versus non-equilibrium phase transition," J. Phys. II **7**, 459–472 (1997).

Shukla, P. and Alam, M., "Nonlinear vorticity-banding instability in granular plane Couette flow: higher-order Landau coefficients, bistability and the bifurcation scenario," J. Fluid Mech. **718**, 131–180 (2013).

Townsend, A. K. and Wilson, H. J., "Frictional shear thickening in suspensions: The effect of rigid asperities," Phys. Fluids **29**, 121607 (2017).

Turing, A. M., "The chemical basis of morphogenesis," Philos. Trans. R. Soc., B **237**, 37–72 (1952).

van Beijeren, H. and Ernst, M. H., *Fundamental Problems in Statistical Mechanics VIII* (North-Holland, Amsterdam, 1994).

Vázquez-Quesada, A., Wagner, N. J., and Ellero, M., "Planar channel flow of a discontinuous shear-thickening model fluid: Theory and simulation," Phys. Fluids **29**, 103104 (2017).

Walgraef, D., *Spatio-Temporal Pattern Formation: With Examples Form Physics, Chemistry and Material Science* (Springer-Verlang, USA, 1996).

Wesfreid, J. E., Brand, H. R., Manneville, P., Albinet, G., and Boccara, N., *Propagation in Systems Far from Equilibrium* (Springer-Verlag, 1987).

Wilson, H. J. and Fielding, S. M., "Linear instability of planar shear banded flow of both diffusive and non-diffusive Johnson–Segalman fluids," J. Non-Newtonian Fluid Mech. **138**, 181–196 (2006).